EDGE DELAMINATION OF COMPOSITE LAMINATES UNDER LOW CYCLE FATIGUE

Nobuhide Uda and Kazuo Kunoo

Department of Aeronautics and Astronautics, Kyushu University
6-10-1 Hakozaki, Higashi-ku, Fukuoka, 812-8581, Japan

SUMMARY: The onset and growth rate of free-edge delamination in composite laminates $[+30_n/-30_n/90_n]_S$ $(n = 1, 2)$ under cyclic loading are quantitatively examined. A critical strain for the onset of the free-edge delamination is predicted using a strain energy release rate. The predicted critical strains are in very good agreement with the experimental results. A linear relation between delamination size and stiffness loss is shown experimentally and analytically. The growth of the delamination in the $[+30_n/-30_n/90_n]_S$ laminates is characterized assuming the delaminations grow in both -30/90 interfaces. The growth rate of the delamination is evaluated with an alternative parameter, stiffness-loss rate during fatigue. The stiffness-loss rate of the delamination is expressed by a power law for the $[+30_n/-30_n/90_n]_S$ laminates.

KEYWORDS: fatigue, delamination, strain energy release rate, free-edge, fracture, toughness, growth rate, stiffness loss

INTRODUCTION

A commonly observed failure mode in composite laminates is delamination between the constituent plies. The delamination, in particular, along a free edge of the composite laminates under in-plane loading has been observed during testing and in service. The free-edge delamination induces redistribution of stresses in the plies of the laminate, and hence stiffness, strength, and fatigue life of the laminate are seriously reduced. A number of experimental and analytical investigations [1-7]*etc.* have been directed toward well understanding free-edge delamination mechanisms. The previous studies have shown that delamination resistance can be characterized quantitatively by applying fracture mechanics. The delamination resistance of composite laminates is evaluated by a critical value of a strain energy release rate (SERR) required to cause the delamination to grow. The objective of this paper is to examine the onset and growth rate of the delamination in composite laminates $[+30_n/-30_n/90_n]_S$. The

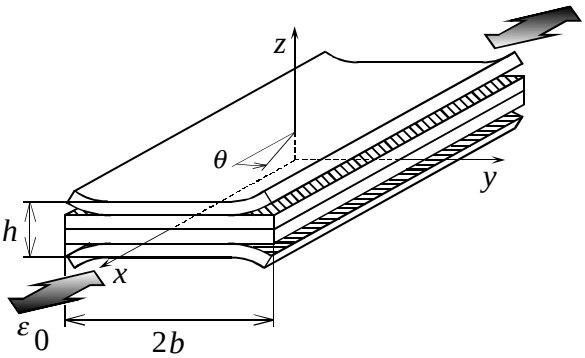

Fig. 1: Free-edge delaminations in composite laminates under cyclic loading.

Table 1: Mechanical properties of AS4/938 and geometry of the specimens.

$E_L = 130\,\text{GPa}$, $E_T = 10\,\text{GPa}$, $G_{LT} = 5.3\,\text{GPa}$, $\nu_{LT} = 0.33$, $\nu_{TT} = 0.30$

$b\,(\text{semi-width}) = 15\,\text{mm}$, $h_0\,(\text{ply thickness}) = 0.15\,\text{mm}$

laminates we experimented with are subjected to uniaxial tensile fatigue as shown in Fig. 1. A critical strain for the onset of the free-edge delamination is predicted using the SERR, and compared with the experimental results. The growth rate of the delamination is evaluated with an alternative parameter, stiffness-loss rate during fatigue.

EXPERIMENTS

Specimens and Apparatus

We conducted low cycle tensile fatigue tests of composite laminates with two types of layups, $[+30/-30/90]_S$ and $[+30_2/-30_2/90_2]_S$. These laminates were made from AS4/938 (Fiberite) graphite-epoxy composite material. Table 1 lists mechanical properties of the material obtained from tension tests, and specimen geometry for the fatigue tests. The fatigue specimens were coupon type similar to ASTM D-3039, and bonded GFRP tabs to the ends. The width and the length between the tabs of the specimens were 30 mm and 170 mm, respectively. The average ply thickness was 0.15 mm. The specimens were tested using a closed-loop hydraulic testing machine, Instron 8501. Table 2 shows conditions and results of the fatigue tests. The stress ratio of the fatigue loading was nearly equal to 0.1, and the frequency was 3 or 5 Hz. The stress maximum of the cyclic loading was chosen to be 40% to 80% to the ultimate tensile strength. We measured strain using strain gages and an extensometer. The strain gages may be fatigued as well as the specimen under the cyclic loading. We hence adopted the extensometer data except when handling of the extensometer had failed. The free edges of the specimens were polished to enhance detection of delamination cracks. The onset and growth of the free-edge delamination were observed using a microscope and a replica technique with an acetate film.

Experimental Results

We interrupted the cyclic loading at specified intervals, and quasi-statically applied 80% load of the cyclic maximum load in order to measure static stiffness of the specimen. Figure 2 shows the stress-strain curves of the $[+30_2/-30_2/90_2]_S$ EQ07-F2 specimen obtained through the quasi-static loading. We got stiffness change during the fatigue test using the initial tangent of the stress-strain curves in Fig. 2. Figure 3 shows stiffness loss and AE (acoustic emission) count rate of the $[+30/-30/90]_S$ EQ02-F2 specimen under the cyclic loading. The stiffness is normalized by the initial tangent modulus of the undamaged specimen. As shown in Table 2,

Table 2: Conditions and results of fatigue test.

Stacking Sequence	Specimen Number	Maximum Stress * [MPa]	Stress Ratio	Test Frequency [Hz]	The Number of Load Cycles at Delamination Onset	The Critical Strain at Delamination Onset	The Number of Load Cycles to Fracture
$[+30/-30/90]_S$	EQ02-F1	241(46%)	0.08	5	100	0.51	21,641
	EQ02-F2	241(46%)	0.08	5	100	0.53	20,200
	EQ02-F3	241(46%)	0.08	5	100	0.51	22,463
	EQ02-F4	216(41%)	0.08	5	100	0.47	91,800
	EQ02-F5	241(46%)	0.08	5	20	0.49	35,750
$[+30_2/-30_2/90_2]_S$	EQ07-F1	150(58%)	0.09	3	100	0.40	67,802
	EQ07-F2	140(54%)	0.09	3	200	0.39	87,548
	EQ07-F6	168(65%)	0.08	3	2	0.38	24,713
	EQ07-F7	181(70%)	0.07	3	1	0.39	20,212

* The figures in the parentheses show the percentage of the maximum stress to the tensile strength.

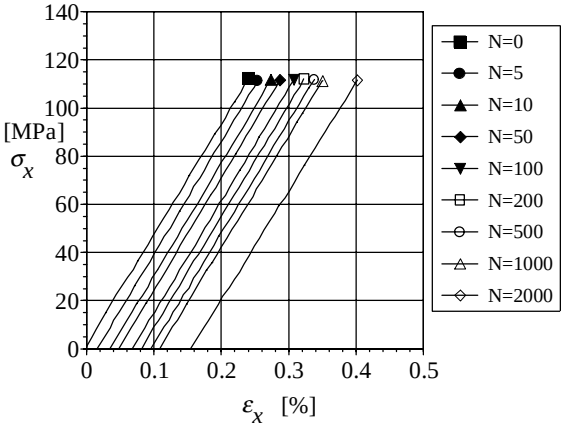

Fig. 2: Stress-strain curves of the $[+30_2/-30_2/90_2]_S$ EQ07F2 specimen obtained from a extensometer.

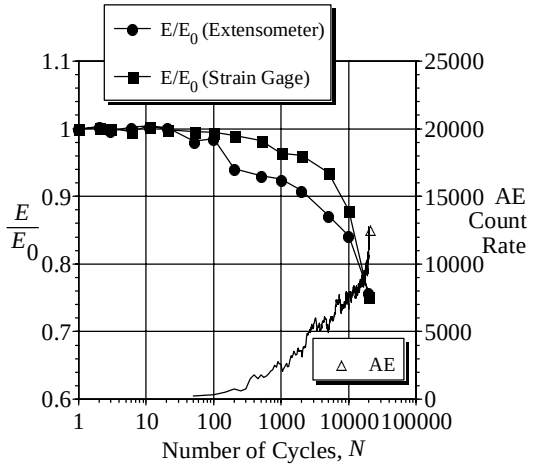

Fig. 3: Stiffness loss and AE count rate of the $[+30/-30/90]_S$ EQ02-F2 specimen under cyclic loading.

the free-edge delamination in the EQ02-F2 specimen occurred at the 100th cycle of loading. The stiffness of the specimen started to reduce and the AE events begun to burst at the loading cycle as shown in Fig. 3.

Fatigue damage of all the laminates was free-edge delamination initiated at the laminate midplane between the two central 90-degree plies. The delamination grew wanderingly between the adjacent –30/90 interfaces and formed a zigzag pattern accompanied with transverse cracks in the 90-degree layer. Figure 4 is a photomicrograph of the replica showing the free-edge delamination in the $[+30/-30/90]_S$ EQ02-F5 specimen at the number of loading cycles $N = 100$.

Fig. 4 : Photomicrograph of the free-edge delamination in the $[+30/-30/90]_S$ EQ02-F5 specimen at $N = 100$.

Only for the $[+30_2/-30_2/90_2]_S$ EQ07 specimens, we observed widthwise growth of the delamination using an ultrasonic C-scan inspection. We inspected 75-mm long area of each specimen. Figure 5 shows C-scan images of the $[+30_2/-30_2/90_2]$s EQ07-F2 specimen at each number of loading cycles. The black region in Fig. 5 shows where delamination has not grown yet, the other gray region depicts where delamination has already occurred. The image of the delaminated area is painted in different shade of gray according to the depth of the delamination. We measured the whole of the delaminated area using an image processing technique. We calculated an average size of the delamination width from dividing the delaminated area by the length of the C-scanned area.

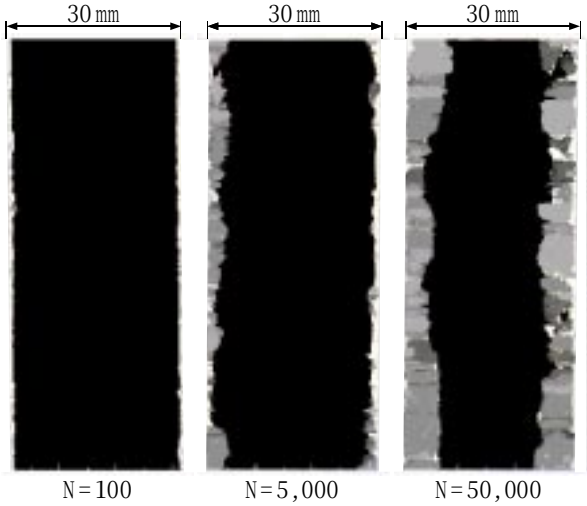

Fig. 5: C-scan images of the $[+30_2/-30_2/90_2]$s EQ07-F2 specimen.

Figure 6 shows the stiffness loss and the delamination size of the $[+30_2/-30_2/90_2]_S$ EQ07-F2 specimen during the cyclic loading. The delamination size is normalized by the semi-width of the specimen. In the case of the

EQ07-F2 specimen, the free-edge delamination was observed at the 200th cycle of loading. Figure 6 shows the stiffness was degraded and the delamination size was increased after $N = 200$.

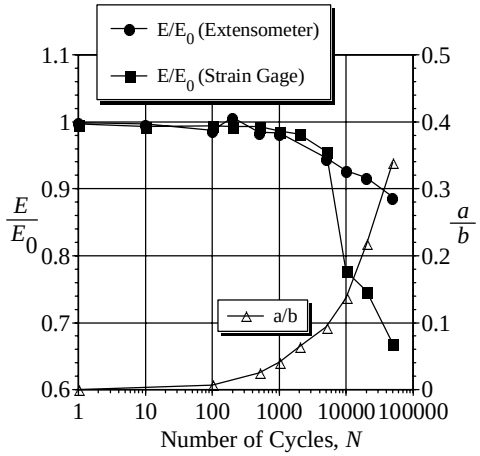

Fig. 6 : Stiffness loss and delamination size of the [+30₂/-30₂/90₂]S EQ07-F2 specimen under cyclic loading.

DISCUSSION

Delamination Onset

A free-edge delamination is usually a mixed-mode failure. A failure criterion for the mixed-mode delamination has been expressed in a form of

$$\left(\frac{G_{\mathrm{I}}}{G_{\mathrm{I_c}}}\right)^p + \left(\frac{G_{\mathrm{II}}}{G_{\mathrm{II_c}}}\right)^q + \left(\frac{G_{\mathrm{III}}}{G_{\mathrm{III_c}}}\right)^r = 1 \ . \qquad (1)$$

where $G_{\mathrm{I_c}}$, $G_{\mathrm{II_c}}$, and $G_{\mathrm{III_c}}$ are the critical values of the Mode-I, Mode-II, and Mode-III SERR, respectively. Wang [8] showed that the SERR converges to a constant value once the delamination had grown one to two ply thicknesses in from the specimen edge. It is commonly accepted that onset of the free-edge delaminations is predicted using the convergent value of the SERR [3,4,8]. The interlaminar fracture data in Ref. [5,7,9] indicate that

$$p = q = r = 1 \ . \qquad (2)$$

The total SERR is written as

$$G_{\mathrm{t}} = G_{\mathrm{I}} + G_{\mathrm{II}} + G_{\mathrm{III}} \ . \qquad (3)$$

We introduce ratios of G_{I}, G_{II} and G_{III} in the total SERR as

$$\xi = G_{\mathrm{I}}/G_{\mathrm{t}} \ , \quad \eta = G_{\mathrm{II}}/G_{\mathrm{t}} \ , \quad \zeta = G_{\mathrm{III}}/G_{\mathrm{t}} \ . \qquad (4)$$

Substituting Eqns (2) and (4) to Eqn (1), we get the critical value of G_{t} as

$$G_{\mathrm{t_c}} = \frac{1}{\left(\xi/G_{\mathrm{I_c}} + \eta/G_{\mathrm{II_c}} + \zeta/G_{\mathrm{III_c}}\right)} \ . \qquad (5)$$

Aoki *et al.* [6,7] pointed out a size effect of the laminate thickness in calculating the SERR as follows.

$$G^{\infty} = \varepsilon_0^{\,2}\, h\, \bar{g}^{\infty} \ , \qquad (6)$$

where G^{∞} is the convergent value of the total SERR for the delamination in the laminate with thickness h, and $\bar{g}^{\infty}$ is the convergent value of the total SERR for the delamination in the laminate with unit thickness under unit applied strain, $\varepsilon_0 = 1$. Using Eqn (6), we get the critical applied strain for the onset of the free-edge delamination in a laminate with an arbitrary thickness as follows.

$$\varepsilon_{0\mathrm{c}} = \sqrt{\frac{G_{\mathrm{t_c}}}{h\,\bar{g}^{\infty}}} \ . \qquad (7)$$

We proposed a generalized quasi-three dimensional classical laminated plate theory (GQ3D-CLT) [10,11] to analyze a laminate with the free-edge delamination. We derived a constitutive equation for a laminate with free-edge delamination as follows.

$$\{N\} = [H]\{C\} \ , \qquad (8)$$

where

$$\{N\}=\sum_{k=1}^{m}\{N\}_{(k)}\ ,\quad \{N\}_{(k)}=\lfloor N_x \quad M_x \quad M_{xy} \quad T_x \rfloor_{(k)}^{T}\ , \tag{9}$$

$$[H]=\sum_{k=1}^{m}[H]_{(k)}\ ,\quad [H]_{(k)}=\begin{bmatrix} a_{11} & b_{11} & b_{16} & c_{11} \\ b_{11} & d_{11} & d_{16} & e_{11} \\ b_{16} & d_{16} & d_{66} & e_{16} \\ c_{11} & e_{11} & e_{16} & f_{11} \end{bmatrix}_{(k)}\ , \tag{10}$$

$$\{C\}=\{C\}_{(1)}=\{C\}_{(2)}=\cdots=\{C\}_{(m)}\ ,\quad \{C\}_{(k)}=\lfloor \varepsilon_0 \quad \kappa_x \quad \kappa_{xy} \quad \omega_x \rfloor_{(k)}^{T}\ . \tag{11}$$

The m in Eqns (9) to (11) is number of sublaminates formed by the delamination. $\{N\}_{(k)}$, $\{C\}_{(k)}$ and $[H]_{(k)}$ are generalized forces, generalized strains and reduced stiffnesses of the k-th sublaminate, respectively. T_x in Eqn (9) is in-plane bending moment and ω_x in Eqn (11) is curvature caused by the T_x. a_{ij}, b_{ij} and d_{ij} in Eqn (10) are reduced extensional stiffness, reduced extension-bending coupling stiffness and reduced bending stiffness, respectively. We can calculate the SERR for the delamination with length a under constant displacement condition as follows.

$$G(a)=-\frac{U(a+\Delta a)-U(a)}{\Delta a}\ , \tag{12}$$

where Δa is a virtual crack extension length, and $U(a)$ is strain energy of the laminate as

$$U(a)=\frac{1}{2}\{N\}\cdot\{C\}\ . \tag{13}$$

We obtain $\bar{g}^{\infty}$ calculating Eqn (12) for the laminate with unit thickness under unit applied strain. Using Eqns (5) and (7) with G_{Ic}, G_{IIc} and G_{IIIc}, we predict the critical value of the nominal strain for the onset of the free-edge delamination under cyclic loading.

On the other hand, O'Brien [3] derived the critical strain for the onset of delamination as follows.

$$\varepsilon_{0\mathrm{c}}=\sqrt{\frac{2\,G_{\mathrm{tc}}}{h\left(E_0-E^{*}\right)}}\ , \tag{14}$$

where E_0 is stiffness of an undamaged laminate calculated from the classical laminated plate theory (CLT), and E^{*} is stiffness of a laminate completely delaminated along one or more interfaces. The stiffness E_0 of a balanced, symmetric composite laminate such as $[+30_n/-30_n/90_n]_S$ is calculated from the CLT as

$$E_0=\frac{1}{X_{11}\,h}\ , \tag{15}$$

where X_{11} is the first element of the inverse extensional stiffness matrix, $\left[A_{ij}\right]^{-1}\ (i,j=1,2,6)$. Applying the rule of mixtures to the completely delaminated laminate, O'Brien obtained the stiffness E^{*} as follows.

$$E^{*}=\frac{\sum_{k=1}^{m}E_k\,t_k}{h}\ , \tag{16}$$

where m is number of the sublaminates formed by the delamination. E_k and t_k are stiffness and thickness of the k-th sublaminate, respectively.

Figure 7 shows the predicted values and the experimental results of the critical strain ε_{0c} for the delamination onset in the $[+30_n/-30_n/90_n]_S$ laminates. The brackets of the experimental results depict the scatter range, and the solid circles represent the mean of several specimens. We predicted ε_{0c} in two ways, using Eqn (7) or Eqn (14). In our experiments, the free-edge delaminations were first observed in the midplane, *i.e.* the 90/90 interface. Since the delamination in the midplane is the mode-I failure, we only need G_{Ic} to calculate Eqn (7).

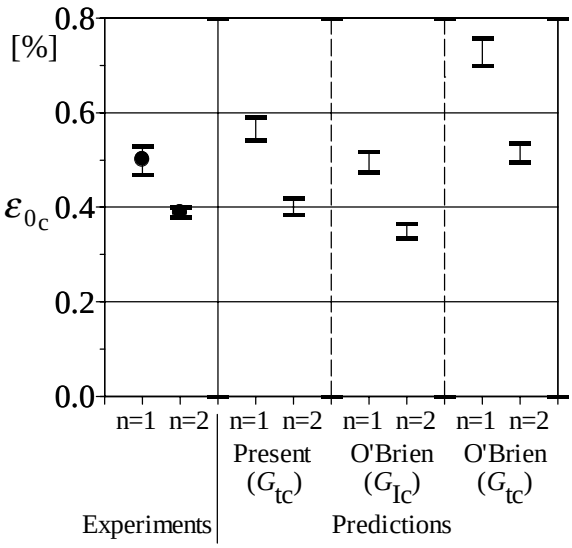

Fig. 7: Critical axial strain for the edge-delamination onset in the $[+30_n/-30_n/90_n]_S$ laminates.

The critical values, G_{Ic}, for materials of the same kind as our composite are reported in Refs. [12,13] as follows.

$$G_{Ic} = 160 - 190 \ [\mathrm{N/m}] \ . \tag{17}$$

The present analysis hence gives ε_{0c} for the 90/90 delamination using Eqn (7) with the following.

$$G_{tc} = G_{Ic} = 160 - 190 \ [\mathrm{N/m}]. \tag{18}$$

The results obtained from the present analysis are plotted at the second column in Fig. 7. Our analytical results are in very good agreement with the experimental results.

O'Brien [3] observed almost the same delamination as shown in Fig. 4 in his specimen [+30/-30/+30/-30/90_3/-30/+30/-30/+30]. He reported the delaminations shifted from one -30/90 interface to another through various 90-degree ply cracks. He analytically modeled these delaminations assuming that the delaminations occur in both -30/90 interfaces. In the case of our specimen $[+30_n/-30_n/90_n]_S$, Eqn (16) becomes the following based on O'Brien's model.

$$E^* = \frac{4E_{(\pm 30)} + 2E_{(90_2)}}{6} \ . \tag{19}$$

He has calculated the stiffness $E_{(\pm 30)}$ neglecting the extension-bending coupling for the [+30/-30] antisymmetric angle-ply sublaminate formed by the delaminations. He explained that the coupling would have been present when only one -30/90 interface had been cleanly delaminated or both -30/90 interfaces had been delaminated at the same time. He hence assumed the delaminations growing in the manner shown in Fig. 4 reduce the effect of the extension-bending coupling.

O'Brien used in Eqn (14) $G_{tc} = 137 \ [\mathrm{N/m}]$ that had been obtained from edge-delamination tests of his specimens. His specimens were made from T300/5208 graphite-epoxy composite material that is similar to our composite material. We believe this critical value of G_t is of G_I, since the value $G_{tc} = 137 \ [\mathrm{N/m}]$ he obtained is nearly equal to Eqn (17). We hence calculated Eqn (14) with Eqns (18) and (19) to predict ε_{0c} using O'Brien's model. The results obtained

using O'Brien's model with $G_{\mathrm{I_c}}$ are depicted at the third column in Fig. 7. The O'Brien's model with $G_{\mathrm{I_c}}$ agrees fairly well with the experiments like as our model.

We analyzed the -30/90 interface delaminations using the generalized quasi-three dimensional finite element method (GQ3D-FEM) developed by the authors [10]. The GQ3D-FEM analysis showed the delaminations in the -30/90 interfaces are the mixed-mode failure with G_{I} and G_{II}. We got the ratios in Eqn (4) from the GQ3D-FEM. The critical values, $G_{\mathrm{II_c}}$, for materials of the same kind as our composite are reported in Refs. [13,14] as follows.

$$G_{\mathrm{II_c}} = 520 - 600 \ [\mathrm{N/m}] \ . \qquad (20)$$

Using Eqns (5), (17) and (20), we estimated the critical value of G_{t} for the mixed-mode delaminations in the -30/90 interfaces as follows.

$$G_{\mathrm{t_c}} = 348 - 407 \ [\mathrm{N/m}] \ . \qquad (21)$$

When we predict ε_{0_c} from O'Brien's model assuming the -30/90 interface delaminations, we should use Eqn (21) for the critical value of G_{t}. We hence calculated Eqn (14) with Eqns (19) and (21) for the O'Brien's model. The results obtained using $G_{\mathrm{t_c}}$ of Eqn (21) are depicted at the last column in Fig. 7. The O'Brien's model with $G_{\mathrm{t_c}}$ overestimates ε_{0_c} in comparison with the experiments.

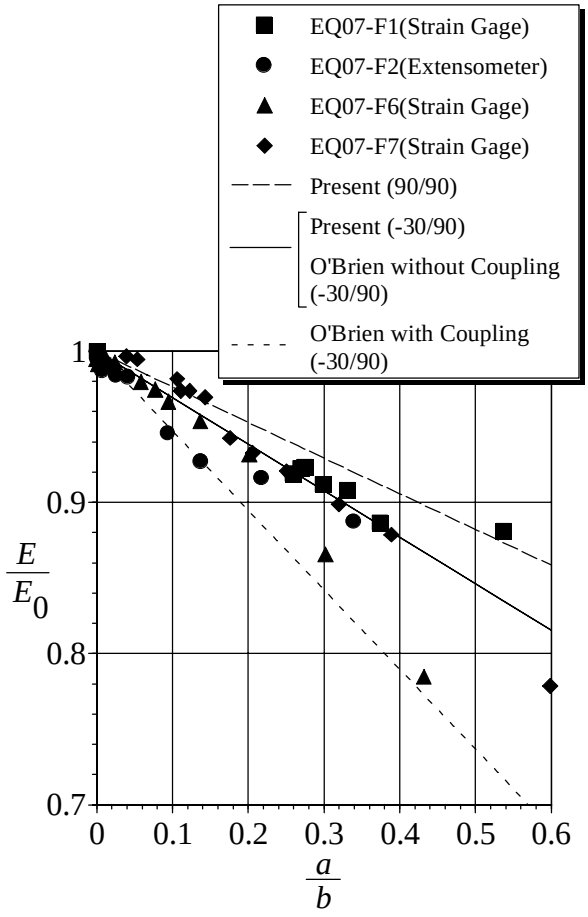

Fig. 8: Relation between delamination size and stiffness of the [+30₂/-30₂/90₂]ₛ EQ07 specimens.

Stiffness Loss

Figure 8 shows relation between the normalized delamination size a/b and the normalized stiffness E/E_0. The experimental results of the $[+30_2/-30_2/90_2]_S$ EQ07 specimens show a roughly linear relation between them. We can calculate the relation between them using the first element of the inverse of the $[H]$ matrix in Eqn (8) for the GQ3D-CLT. Assuming the delamination grows only in the 90/90 interface, we got the dash line in Fig. 8. Postulating the delaminations grow in both -30/90 interfaces, we obtained the solid line in Fig. 8. The postulate of the -30/90 interface delaminations gives a very good agreement with the experimental results. The growth of the delaminations in the $[+30_n/-30_n/90_n]_S$ specimens is characterized using the GQ3D-CLT with the -30/90 interface delaminations.

On the other hand, O'Brien [3] derived the stiffness of a laminate with delamination size a as follows.

$$E = \left(E^* - E_0\right)\frac{a}{b} + E_0 \ . \qquad (22)$$

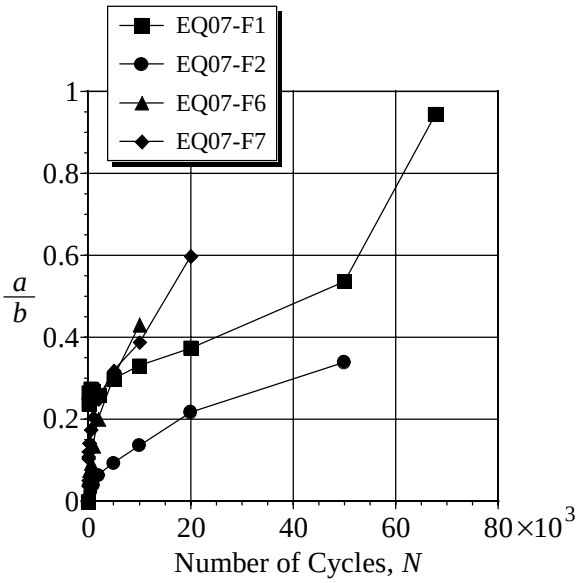

Fig. 9: Delamination size as a function of load cycles obtained from the experiments of the [+30₂/-30₂/90₂]$_S$ EQ07 specimens.

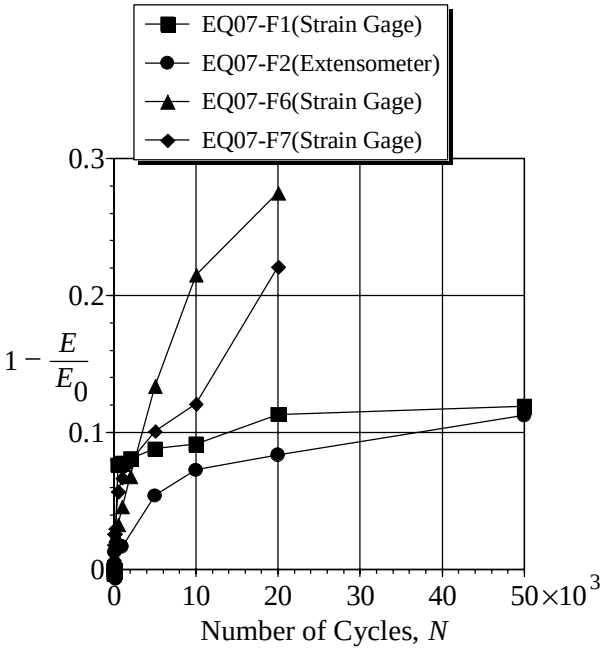

Fig. 10: Stiffness loss as a function of load cycles obtained from the experiments of the [+30₂/-30₂/90₂]$_S$ EQ07 specimens.

As we mentioned before, O'Brien has calculated the stiffness $E_{(\pm 30)}$ neglecting the extension-bending coupling. Applying Eqn (22) without the coupling to the laminates in which the delaminations grow at both -30/90 interfaces, we got the same result as the GQ3D-CLT for the -30/90 interface delaminations as shown in Fig. 8. Calculation of Eqn (22) with the coupling gave the dotted line in Fig. 8. The O'Brien's model with the coupling disagrees with the experiments. Applying Eqn (22) without the coupling to the laminate in which the delamination grows only at the 90/90 interface, we obtained $E^* = E_0$. Calculation of Eqn (22) without the coupling hence gives that the stiffness has never decreased if a delamination might grow only in the 90/90 interface.

Delamination-Growth Rate

Figure 9 shows a plot of normalized delamination size as a function of load cycles obtained from the experiments of the [+30₂/-30₂/90₂]$_S$ EQ07 specimens. As depicted in Fig. 9, once the delaminations had grown over the entire length of the specimen edge, the delamination size linearly increased with the load cycles. Just before fracture of the specimen, the delamination rapidly grew across the laminate width like the EQ07-F1 shown in Fig. 9. We define a growth rate, da/dN, of the delamination using a gradient of the linear region in Fig. 9.

There is a linear relation between the stiffness loss and the delamination size as shown in Fig. 8. We hence expect the stiffness loss should be interrelated with the load cycles as well. Figure 10 shows relation between the load cycles and the stiffness loss. As expected, we can see a fairly linear region once the delamination had grown away from the edge, and define a stiffness-loss rate dE/dN.

We calculated the delamination-growth rates and the stiffness-loss rates applying a least-squares linear approximation to the linear regions in Figs. 9 and 10, respectively. We estimated then amplitudes of the total SERR, ΔG, from Eqn (6) using the amplitudes of the applied strain in the linear regions of Figs. 9 and 10. As we mentioned before, the growth of

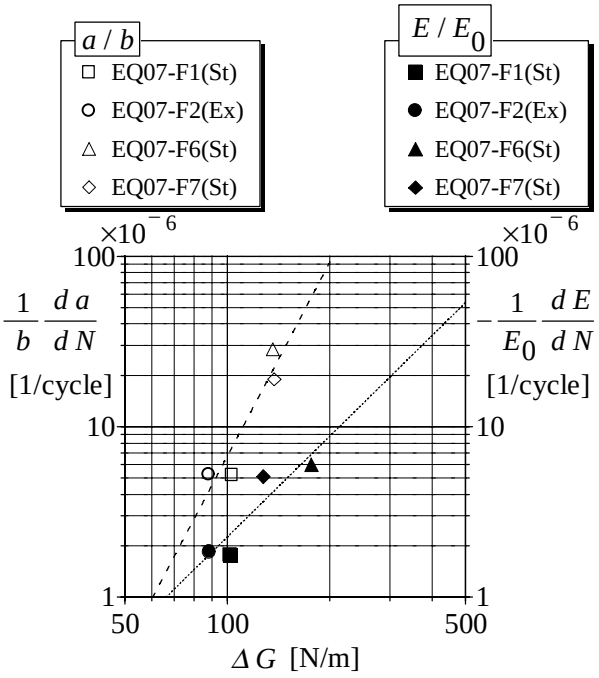

Fig. 11: Power law curve fits for delamination-growth rate and stiffness-loss rate of the $[+30_2/-30_2/90_2]_S$ EQ07 specimens. .

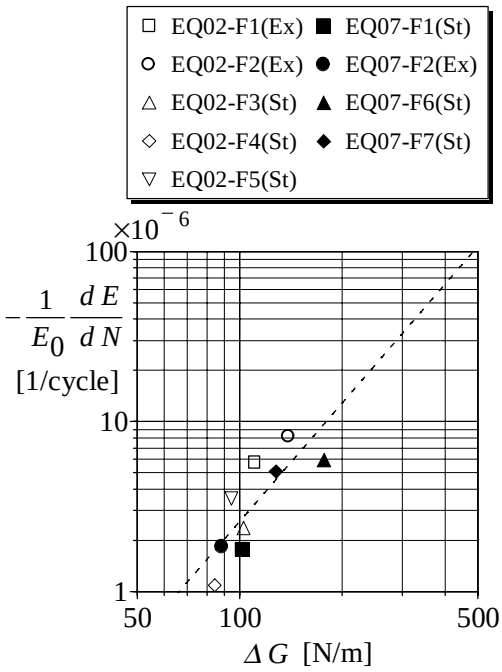

Fig. 12: Stiffness-loss rate of the $[+30/-30/90]_S$ EQ02 and $[+30_2/-30_2/90_2]_S$ EQ07 specimens. .

the delaminations in the $[+30_2/-30_2/90_2]_S$ EQ07 specimens is characterized using the GQ3D-CLT with the -30/90 interface delaminations. We hence obtained ΔG assuming the free-edge delaminations grow in both -30/90 interfaces. Figure 11 shows da/dN or dE/dN as a function of ΔG for the $[+30_2/-30_2/90_2]_S$ EQ07 specimens. These plots indicate the delamination-growth rate and the stiffness-loss rate fit excellently power laws of forms as

$$\frac{1}{b}\frac{da}{dN} = \alpha \Delta G^{\beta} \text{ and } -\frac{1}{E_0}\frac{dE}{dN} = \varphi \Delta G^{\psi} \ . \tag{23}$$

The stiffness-loss rate is a useful parameter as pointed out by O'Brien [3] since it could be estimated without measuring the delamination size directly.

We obtained the stiffness-loss rates of the $[+30/-30/90]_S$ EQ02 specimens, too. Figure 12 depicts the stiffness-loss rates of the EQ02 and EQ07 specimens. It shows that the growth of the delaminations is expressed by the same power law of the stiffness-loss rate for the $[+30_n/-30_n/90_n]_S$ laminates no matter how much the layer thickness n is.

Applying a least-squares fit to the experimental results in Fig. 11, we got the power law for the delamination-growth rate in $[+30_2/-30_2/90_2]_S$ EQ07 specimens as follows.

$$\frac{1}{b}\frac{da}{dN} = 1.82\times10^{-13}\Delta G^{3.78} \ . \tag{24}$$

In Fig. 12, we obtained the power law for the stiffness-loss rate in the $[+30/-30/90]_S$ EQ02 and $[+30_2/-30_2/90_2]_S$ EQ07 specimens as follows.

$$-\frac{1}{E_0}\frac{dE}{dN} = 6.11\times10^{-11}\Delta G^{2.31} \ . \tag{25}$$

CONCLUTIONS

1. We predicted a critical strain for onset of free-edge delamination in $[+30_n/-30_n/90_n]_S$ $(n = 1, 2)$ laminates under cyclic loading, using the SERR. The predicted strains were in very good agreement with our experimental results.
2. A linear relation between stiffness loss and delamination size was found in the experiments of the $[+30_n/-30_n/90_n]_S$ laminates under cyclic loading. The stiffness loss was calculated assuming the delaminations grew in both -30/90 interfaces. The analytical results agreed with the experiments very well.
3. Growth of free-edge delaminations in $[+30_n/-30_n/90_n]_S$ laminates was characterized by developing a power law correlation between amplitude of the SERR and stiffness-loss rate. The results of the experiments show the growth of the delaminations is expressed by the same power law for the $[+30_n/-30_n/90_n]_S$ laminates no matter how much the layer thickness n is.

REFERENCES

[1] Pipes,R.B. and Pagano,N.J., "Interlaminar Stresses in Composite Laminates Under Uniform Axial Extension," Journal of Composite Materials, Vol.4, 1970, pp.538-548.

[2] Wang,A.S.D. and Crossman,F.W., "Initiation and Growth of Transverse Cracks and Edge Delamination in Composite Laminates, Part 1. An Energy Method," Journal of Composite Materials Supplement, Vol.14, 1980, pp.71-87.

[3] O'Brien,T.K., "Characterization of Delamination Onset and Growth in a Composite Laminate," ASTM STP 775, 1982, pp.140-167.

[4] O'Brien,T.K., "Mixed-Mode Strain-Energy-Release Rate Effects on Edge Delamination of Composites," ASTM STP 836, 1984, pp.125-142.

[5] O'Brien,T.K., Johnston,N.J., Raju,I.S., Morris,D.H. and Simonds,R.A., "Comparisons of Various Configurations of the Edge Delamination Test for Interlaminar Fracture Toughness," ASTM STP 937, 1987, pp.199-221.

[6] Aoki,T., and Kondo,K., "Free-Edge Delamination of Anisotropic Composite Laminates, (I) Theoretical Approach," Journal of the Japan Society for Aeronautical and Space Sciences, Vol.37, 1989, pp.29-38.

[7] Aoki,T., Kubo,T. and Kondo,K., "Free-Edge Delamination of Anisotropic Composite Laminates, (II) Experimental Approach," Journal of the Japan Society for Aeronautical and Space Sciences, Vol.37, 1989, pp.144-154.

[8] Wang,S.S., "Edge Delamination in Angle-Ply Composite Laminates," AIAA Journal, Vol.22, No.2, 1984, pp.256-264.

[9] Johnson,W.S. and Mangalgiri,P.D., "Influence of the Resin on Interlaminar Mixed-Mode Fracture," ASTM STP 937, 1987, pp.295-315.

[10] Kunoo,K., Uda,N., Ono,K. and Onohara,K., "Generalized Quasi-Three Dimensional Analysis of Composite Laminates with Unsymmetrically Located Free-Edge Delaminations," Theoretical and Applied Mechanics, Vol.41, 1992, pp.137-146.

[11] Uda,N., Kunoo,K. and Kim,I.K., "A Simplified Method for Determining the Strain Energy Release Rate Components of Free-Edge Delaminations in Composite Laminates," Proceedings of ICCM-10, Vol.1, 1995, pp.237-244.

[12] Whitney,J.M. and Knight,M., "A Modified Free-Edge Delamination Specimen," ASTM STP 876, 1985, pp.298-314.

[13] Prel,Y.J., Davies,P., Benzeggagh,M.L. and de Charentenay,F.-X., "Mode I and Mode II Delamination of Thermosetting and Thermoplastic Composites," ASTM STP 1012, 1989, pp.251-269.

[14] Corleto,C.R. and Bradley,W.L., "Mode II Delamination Fracture Toughness of Unidirectional Graphite/Epoxy Composites," ASTM STP 1012, 1989, pp.201-221.